Fast and slow components of the extratropical atmospheric circulation response to CO_2 forcing

Paulo Ceppi*, Giuseppe Zappa, and Theodore G. Shepherd

Department of Meteorology, University of Reading, Reading, United Kingdom

Jonathan M. Gregory

NCAS-Climate, University of Reading, Reading, and Met Office Hadley Centre, Exeter, United Kingdom

**Corresponding author address:* Department of Meteorology, University of Reading, Earley Gate, P.O. Box 243, Reading RG6 6BB, United Kingdom

E-mail: p.ceppi@reading.ac.uk

ABSTRACT

Poleward shifts of the extratropical atmospheric circulation are a common response to CO_2 forcing in global climate models (GCMs), but little is known about the time dependence of this response. Here it is shown that in coupled climate models, the long-term evolution of sea surface temperatures (SSTs) induces two distinct time scales of circulation response to step-like CO_2 forcing. In most Coupled Model Intercomparison Project phase 5 GCMs as well as in the multi-model mean, all of the poleward shift of the midlatitude jets and Hadley cell edge occurs in a fast response within 5 to 10 years of the forcing, during which less than half of the expected equilibrium warming is realized. Compared with this fast response, the slow response over subsequent decades to centuries features stronger polar amplification (especially in the Antarctic), enhanced warming in the Southern Ocean, an El Niño-like pattern of tropical Pacific warming, and weaker land-sea contrast. Atmosphere-only GCM experiments demonstrate that the SST evolution drives the difference between the fast and slow circulation responses, although the direct radiative effect of CO_2 also contributes to the fast response. It is further shown that the fast and slow responses determine the long-term evolution of the circulation response to warming in the RCP4.5 scenario. The results imply that shifts in midlatitude circulation generally scale with the radiative forcing, rather than with global-mean temperature change. A corollary is that time slices taken from a transient simulation at a given level of warming will considerably overestimate the extratropical circulation response in a stabilized climate.

1. Introduction

A well-known feature of the atmospheric circulation response to CO_2 forcing is the overall poleward shift of extratropical circulation, including the jet streams (Kushner et al. 2001; Yin 2005; Barnes and Polvani 2013), the storm tracks (Chang et al. 2012; Harvey et al. 2014), and the edge of the tropics (Lu et al. 2007; Kang and Polvani 2011; Ceppi et al. 2013). This poleward shift is primarily mediated by sea surface temperature (SST) changes, as demonstrated by climate model experiments forced only with a prescribed SST increase (Brayshaw et al. 2008; Staten et al. 2012; Grise and Polvani 2014), although the direct effect of CO_2 (in the absence of any SST changes) also contributes to the poleward circulation shift (Deser and Phillips 2009; Staten et al. 2012; Grise and Polvani 2014).

In previous analyses of atmospheric circulation change under greenhouse gas forcing, the circulation response is typically defined as the difference in climatology between a control present-day (or pre-industrial) state, and a future warmer state. While convenient, such a definition conceals any possible time dependence of the forced circulation response. Since circulation shifts are mainly driven by increasing SST, a simple, naïve assumption is that the circulation will shift at the same rate as global-mean warming over the course of the transient response to greenhouse gas forcing. A related assumption that spatial patterns of climate response scale with global-mean temperature change, known as "pattern scaling," is commonly made for temperature and precipitation, for example when estimating regional climate responses under scenarios for which no global climate model (GCM) simulations are available (e.g., Santer et al. 1990; Mitchell 2003; Tebaldi and Arblaster 2014, and references therein).

It is known, however, that transient patterns of SST response evolve over time following CO_2 forcing – in violation of the pattern scaling assumption – primarily because the ocean system includes processes characterized by multiple time scales. In particular, GCMs forced with an abrupt CO_2 increase show that SST anomalies in regions such as the Southern Ocean, the North Atlantic, and the tropical Pacific substantially deviate from linearity with respect to global-mean warming over the course of the transient response (Manabe et al. 1990, 1991; Stouffer 2004; Held et al. 2010; Armour et al. 2013; Geoffroy and Saint-Martin 2014; Long et al. 2014; Rugenstein et al. 2016b). Since the extratropical circulation response depends sensitively on the spatial pattern of warming (e.g., Butler et al. 2010; Chen et al. 2010; Harvey et al. 2014; Ceppi et al. 2014), this suggests that midlatitude circulation changes may be characterized by multiple time scales, and may not generally scale with global-mean temperature change. The impact of the evolution of SSTs on the time scales of circulation change would be in addition to the previously identified rapid dynamical adjustment to CO_2 forcing, which acts on a time scale of weeks to months (Deser and Phillips 2009; Staten et al. 2012; Wu et al. 2013; Bony et al. 2013; Grise and Polvani 2014, 2017).

In this paper we demonstrate that the SST-mediated midlatitude circulation response to CO_2 forcing involves two distinct time scales, which can be explained by time-evolving patterns of SST change. In the majority of CMIP5 GCMs and in the multi-model mean, all of the poleward shift occurs in a fast response (including the direct CO_2 response) within 5 to 10 years of the forcing. To demonstrate the existence of distinct time scales of atmospheric circulation change, we analyze abrupt CO_2 forcing CMIP5 experiments (section 3), which provide the best possible separation between the various time scales of climate response to radiative forcing. In section 4, we then show that the same time scales of response also operate in RCP4.5, a scenario with gradually increasing forcing. Finally, we summarize and discuss our results in section 5.

2. Data and Methods

a. Climate model experiments

Most of the results presented in this paper are based on CMIP5 coupled atmosphere-ocean GCM experiments (Taylor et al. 2012). The atmospheric circulation response to warming is assessed in 28 140-year abrupt4$\times CO_2$ simulations, in which atmospheric CO_2 concentration is instantaneously quadrupled relative to pre-industrial values at the start of year 1, then held constant. Climate anomalies are calculated by subtracting the parallel reference pre-industrial control integration from the abrupt4$\times CO_2$ simulation, to remove any model drift. Monthly-mean fields are aggregated into annual-mean values prior to analysis. The models included in the analysis are listed in Table 1.

By the end of the 140-year abrupt4$\times CO_2$ experiments, climate has not yet reached a steady state due to the long equilibration time scale of the ocean. To explore the relationship between circulation change and warming on time scales longer than 140 years, we use an ensemble of coupled abrupt4$\times CO_2$ integrations of the Community Earth System Model (CESM; Hurrell et al. 2013) with the atmospheric component CAM4 (Neale et al. 2010) extending to 1000 years, described in Rugenstein et al. (2016a). The ensemble includes 121 members during the first two years, 13 members between years 3 and 100, 6 members between years 101 and 250, and 1 member for the remainder of the integration. The ensemble members are branched off in January of subsequent years of the reference pre-industrial simulation. We use only the ensemble mean in our analysis.

In addition to these coupled simulations, we also perform atmosphere-only CAM4 experiments with imposed patterns of SST change, designed to understand the role of time-varying patterns of surface warming for the circulation response. These experiments are run for 25 years after 1 year of spin-up. Both the coupled and the atmosphere-only integrations are performed at a resolution of 1.9° latitude by 2.5° longitude with 26 vertical levels.

b. Atmospheric circulation metrics

In this paper we focus on meridional shifts of the zonal-mean circulation, quantified by indices of jet latitude and poleward edge of the Hadley cells. The jet latitude is calculated separately for the Southern Hemisphere, the North Pacific basin (140° E to 120° W), and the North Atlantic/European sector (60° W to 60° E). Jet latitude is defined as a centroid of the 850 hPa zonal wind distribution between 30° and 60°,

$$\phi_{\text{jet}} = \int_{30^\circ}^{60^\circ} \phi \bar{u}^2 \, d\phi \Bigg/ \int_{30^\circ}^{60^\circ} \bar{u}^2 \, d\phi,$$

where ϕ is latitude and the overbar denotes a zonal average; latitudes with climatological easterlies are excluded from the calculation. Using the square of the zonal wind ensures that more weight is given to latitudes of strong westerly wind. Similar jet definitions have been used in previous literature (Chen et al. 2008; Ceppi et al. 2014). For the Hadley cell edge, we use the latitude where the meridional mass streamfunction crosses zero in the subtropics at 500 hPa, after cubically interpolating the values onto a 0.1° latitude grid. Note that very similar results are obtained if the latitude of zero surface zonal-mean zonal wind in the subtropics is used instead as a measure of the Hadley cell edge, as in Vallis et al. (2015) (not shown). All shifts are defined as positive poleward.

3. Circulation response to abrupt CO_2 forcing

a. Two time scales of climate response

Plotting jet latitude against global-mean temperature anomaly reveals the existence of two distinct time scales of atmospheric circulation response to CO_2 forcing in abrupt4×CO_2 experiments

(Fig. 1). Following CO_2 quadrupling, the multi-model mean jets rapidly shift poleward with increasing temperature during the first few years of the integrations. However, the shifting tends to cease after about 5 years, despite steadily increasing global-mean temperature; the mean trend even reverses in the North Pacific basin, where the zonal-mean jet returns to its original latitude by the end of the abrupt4$\times CO_2$ simulations. Henceforth we define the "fast" and "slow" circulation responses as the changes between the control climate and the mean of years 5–10, and between years 5–10 and 121–140, respectively (black crosses in Fig. 1). During the fast response, the planet warms by 3.0 K on average, less than half the expected equilibrium warming of 6.6 K based on estimated forcing and feedback values in our set of GCMs (Caldwell et al. 2016).

Despite considerable inter-model spread in jet shift, as evidenced by the 75% intervals in Fig. 1, the tendency for a weaker poleward shift in the slow response is robust across climate models (Fig. 2). In the Southern Hemisphere (SH), this difference is present in all of the models; and while the circulation systematically shifts poleward in the fast response, the shifts are as often positive as negative in the slow response, with no shift in the multi-model mean. In the Northern Hemisphere (NH), the spread is larger but only a few models show a more positive shift in the slow response. The Hadley cell edge response is consistent with that of the midlatitude jets, suggesting that coherent changes in large-scale circulation sensitivity to warming occur between the fast and slow responses.

The direct response to CO_2 forcing, occurring on a time scale of weeks to months, is part of the fast response as defined here and may partly account for the nonlinear relationship between circulation shifts and global-mean temperature identified in Figs. 1 and 2 (Staten et al. 2012; Wu et al. 2013; Grise and Polvani 2014, 2017). However, this effect should be restricted to year 1, and therefore cannot account for the bulk of the circulation shift by years 5–10 (Fig. 1). To understand the time scales of atmospheric circulation shifts, we therefore turn to the evolution of patterns of SST change during the transient response to CO_2 forcing (e.g., Manabe et al. 1990; Held et al. 2010; Long et al. 2014). The evolution of SST patterns could have implications for changes in baroclinicity (i.e. meridional temperature gradients and vertical stability), important for midlatitude circulation shifts. We investigate this possibility in the next subsection by considering the joint evolution of the patterns of surface temperature and zonal wind response.

b. Spatial patterns of temperature and zonal wind response

The multi-model mean fast and slow patterns of surface air temperature change, and the corresponding 850 hPa zonal wind anomaly patterns, are shown in Fig. 3. Evident differences are visible between the fast and slow warming patterns, which are robust across models (stippled regions in Fig. 3). Part of these differences are consistent with the rapid adjustment to CO_2 forcing (taking place during the first few weeks to months following the CO_2 increase), associated with enhanced warming over land relative to ocean areas in the fast response. Large differences in warming pattern between fast and slow responses also occur over the ocean, however, reflecting differences in the pattern of SST change. The Southern Ocean particularly stands out due to strongly suppressed warming in the fast response relative to the global mean, while in the slow response it warms on par with the global average. Instead of the interhemispheric gradient found in the fast response, the slow response pattern is generally characterized by a more hemispherically symmetric SST increase, with a tendency toward an El Niño-like pattern in the tropical Pacific (Collins et al. 2005; Kohyama and Hartmann 2016), slightly suppressed subtropical warming relative to the global mean, and suppressed warming in the North Atlantic, due to a weakening of the meridional overturning circulation in that ocean basin (Drijfhout et al. 2012; Collins et al. 2013). The slow response pattern also features a higher degree of polar amplification compared with the fast response, particularly over the Antarctic cap.

The differences between fast and slow temperature and circulation responses are consistent with the understanding that the ocean thermodynamic response to forcing is dominated by two time scales: a fast time scale of a few years associated with the coupled atmosphere–mixed-layer ocean system, and a much slower time scale (of the order of 100 years) determined by the large heat capacity of the deep ocean (Dickinson 1981; Manabe et al. 1990; Gregory 2000; Held et al. 2010; Olivié et al. 2012; Geoffroy et al. 2013). While the distinction between time scales of mixed-layer and deep ocean warming offers a plausible explanation for the time dependence of SST warming patterns, various additional processes also contribute to local SST changes, including the climatological ocean circulation (Armour et al. 2016), changes in ocean circulation (Drijfhout et al. 2012; Woollings et al. 2012), and coupled air-sea feedbacks (Bjerknes 1969; Xie and Philander 1994; Clement et al. 1996; Xie et al. 2010), to name a few. As an additional caveat, the time scales of ocean heat uptake may well vary regionally, so that the evolution of SSTs cannot be entirely captured by two time scales only. Understanding the evolution of transient SST anomaly patterns is beyond the scope of this work, but we note that the fast and slow warming patterns in Fig. 3 are highly consistent with those documented in previous work in different sets of GCMs (Held et al. 2010; Geoffroy and Saint-Martin 2014; Long et al. 2014), suggesting that the processes underlying the time dependence of SST patterns are reasonably robust across GCMs.

The fast and slow zonal wind response patterns (right column of Fig. 3) reflect the evolution of jet latitude seen in Fig. 1: while the jets shift poleward in all regions in the fast response, a weak equatorward jet shift is visible in the North Pacific in the slow response, with little change in extra-tropical zonal wind elsewhere. To understand the relationship between circulation responses and warming patterns, it is helpful to consider the patterns in Fig. 3 along with the vertical structure of the changes in zonal-mean temperature and wind shown in Fig. 4. First focusing on the SH, we note that in the fast response, the delayed Southern Ocean warming causes an anomalously strong meridional temperature gradient across the midlatitudes throughout the troposphere (Fig. 4a), favoring a strengthening and poleward shift of the eddy-driven jet (Butler et al. 2010; Chen et al. 2010; Harvey et al. 2014; Ceppi and Hartmann 2016). By contrast, the slow warming pattern is associated with a clear weakening of the meridional temperature gradient at lower and middle tropospheric levels, due to amplified Antarctic warming, which alone would favor an equatorward jet shift (Butler et al. 2010). The lack of a clear SH zonal wind response to the slow warming reflects cancelling effects of upper- and lower-level temperature gradient changes (Harvey et al. 2014; Ceppi and Hartmann 2016).

In the NH, the weaker fast jet response in the NH relative to the SH is consistent with the effect of amplified Arctic warming on midlatitude baroclinicity (Fig. 4a,c). In the slow response, warming becomes more muted in the subtropics to midlatitudes, so that the low-level temperature gradient across the midlatitudes weakens further, which may contribute to the slight equatorward shift of the zonal-mean circulation (Fig. 4b,d). However, zonal asymmetries in warming may also contribute substantially to the NH jet and stationary wave response (Delcambre et al. 2013; Simpson et al. 2014). In particular, the slow warming pattern includes an El Niño-like component in the tropical Pacific (Fig. 3b) which may contribute to the North Pacific jet response. In the next subsection, we demonstrate that the SST anomaly patterns are primarily responsible for the differences between fast and slow temperature and zonal wind responses.

c. Relative roles of direct and SST-mediated effects of CO_2

To confirm the key role of surface warming patterns for differences in circulation sensitivity to warming, and to disentangle the contributions of the direct component of CO_2 forcing and SST change to the atmospheric circulation response, we perform atmosphere-only GCM (AGCM) experiments in which we separately impose the multi-model mean fast SST change, the slow SST change, and the CO_2 increase while keeping SSTs unchanged. The perturbed SST experiments also include the corresponding changes in sea ice cover. Climate responses are calculated relative to an experiment with SSTs and sea ice taken from the pre-industrial control CMIP5 multi-model mean.

We first consider the bottom two rows of Fig. 5, which can be directly compared with Fig. 4. When forced with the multi-model mean SST and CO_2 changes[1], our AGCM produces temperature and zonal wind changes in close agreement with the CMIP5 model mean. In particular, it recovers the large difference in jet sensitivity to global warming between the fast and slow response. The fast response can be further decomposed into contributions of direct radiative forcing of CO_2 and SST changes (top two rows of Fig. 5). This reveals that SST changes account for most of the tropospheric temperature changes and SH jet shift in the fast response; however, the direct effect of CO_2 also causes a poleward jet shift in both hemispheres, associated with tropospheric warming (particularly over NH landmasses) and strong stratospheric cooling. Note that the direct effect of CO_2 on circulation seems to be larger in this AGCM compared with most CMIP5 models (cf. the year 1 response in Fig. 1 and Grise and Polvani 2014).

d. Centennial changes in temperature and circulation

Because the ocean takes centuries to equilibrate with the imposed greenhouse gas forcing, the model climates have not reached equilibrium by the end of the CMIP5 abrupt4$\times CO_2$ experiments. Consequently, the patterns of temperature and circulation response continue evolving after year 140 of the experiment. We investigate the centennial circulation response using a 1000-year abrupt4$\times CO_2$ experiment with CESM (section 2a). As shown in Fig. 6, the relationship between

[1]Note that the fast SST and CO_2 changes are imposed in separate experiments, and the responses are added to obtain the combined effect in Fig. 5c,g. Previous work suggests that these responses are approximately additive (Deser and Phillips 2009; Staten et al. 2012).

jet shift and global-mean temperature in CESM is in good qualitative agreement with the mean CMIP5 model behavior: the jets shift poleward during the first few years of the integration, following which the jet latitude stabilizes – or decreases in the case of the North Pacific jet. The main differences relative to the CMIP5 ensemble are (a) larger North Pacific jet fast and slow responses, (b) a weaker SH jet shift, and (c) a shorter time scale for the fast response (the peak jet latitude being reached by year 2 or 3).

Warming patterns being specific to each model, it is unsurprising that CESM's fast and slow temperature and zonal wind patterns present differences relative to CMIP5 models (top two rows of Fig. 7, vs. Fig. 3). In the fast (subdecadal) temperature response, Southern Ocean warming is less suppressed compared with the CMIP5 ensemble, and larger zonal asymmetries are present in the tropics. These features are consistent with a weak SH jet shift, and with a large tropical zonal wind response that is absent from the CMIP5 multi-model mean (Fig. 7a,d). Nevertheless, clear similarities are also visible in the temporal evolution of these patterns: as in CMIP5, the slow response shows a transition to a more hemispherically symmetric temperature pattern, with delayed Antarctic and Southern Ocean warming and an El Niño-like pattern of SST anomalies in the tropical Pacific in the slow (decadal) response.

Beyond year 140 of the abrupt4$\times$$CO_2$ experiment, the patterns of temperature and zonal wind response continue evolving (the centennial response in Fig. 7c,f). The surface warming pattern becomes increasingly hemispherically and zonally symmetric, being mainly characterized by polar amplification. This favors a slight weakening of the midlatitude westerlies, particularly in the SH and in the North Atlantic. The weak overall changes in extratropical winds once again suggest canceling effects between polar-amplified warming at low levels, and tropically-amplified warming aloft, causing meridional temperature gradient changes of opposite sign. Taken together, Figs. 6 and 7 suggest that the circulation response to CO_2 forcing is primarily determined by the changes occurring during the first 140 years following the forcing; the very slow warming on time scales of centuries to millennia does not strongly change the nature of the dynamical response, particularly in the extratropics, and does not cause further poleward circulation shifts. However, since the ocean processes controlling long-term warming patterns remain poorly understood and are likely to vary across models, this result will need to be further tested with other coupled GCMs.

4. Fast and slow circulation responses in RCP4.5

a. Relationship between step and gradual forcing experiments

The abrupt4$\times$$CO_2$ experiments considered so far are helpful in understanding the relationship between atmospheric circulation and global-mean temperature anomaly because they provide an optimal time scale separation and a good signal-to-noise ratio thanks to the large forcing. However, this understanding is interesting mainly to the extent that it can be applied to more realistic gradual forcing scenarios. If the climate responses are linear in forcing magnitude, then any greenhouse gas forcing experiment can be understood as consisting of a sum of responses to small abrupt CO_2 forcings at various time scales (Good et al. 2011, 2013). Linearity in forcing magnitude has been shown to hold to a good approximation for the temperature response (Good et al. 2013), meaning that the gradual forcing responses can be traced back to abrupt experiments. In this section, we demonstrate that the two time scales of circulation response identified in abrupt4$\times$$CO_2$ integrations are also expressed in gradual forcing experiments, causing a decrease in the tendency for the circulation to shift poleward with warming as greenhouse gas concentrations stabilise and climate approaches equilibrium.

To test the applicability of our findings to realistic future scenarios, we consider the RCP4.5 experiment in CMIP5, for which 12 GCMs have provided long integrations reaching year 2299 (Table 1). We select this experiment because the anthropogenic forcing agent concentrations are stabilized relatively early in the experiment (around year 2080, compared with year 2250 in RCP8.5), offering a chance to detect the various time scales of temperature and circulation response in the experiment. Although the anthropogenic forcing peaks even earlier in RCP2.6 (around 2050), the small magnitude of the forcing compared with RCP4.5 makes it more difficult to separate the signal from the noise in the dynamical response.

The time series of the sum of anthropogenic forcing agents (expressed as CO_2-equivalent concentrations in ppm; Meinshausen et al. 2011) and global-mean surface air temperature anomaly relative to 1900–1949 are shown in Fig. 8 (black curves). The total concentration of anthropogenic forcing agents (dominated by CO_2) quickly rises between the late twentieth century and about 2080, after which it remains approximately stable. Consistent with this, global-mean temperature rises rapidly until the late twenty-first century, but continues increasing more slowly for the following two centuries as the deep ocean slowly adjusts to the forcing.

To relate the RCP4.5 responses to the abrupt4$\times$$CO_2$ experiments, a few assumptions are necessary. In addition to assuming that the response is linear in forcing magnitude, we make the simplification that the response to abrupt CO_2 forcing can be fully characterized by a combination of the two patterns identified in section 3a. We also make the further assumption that all anthropogenic forcing agents produce the same patterns of response as CO_2. This assumption is likely to be inaccurate in the case of aerosol forcing, whose warming patterns are distinct from those induced by CO_2 (Wang et al. 2016) – even though the patterns also include common features due to similar ocean-atmosphere feedbacks (Xie et al. 2013). To the extent that the above assumptions are true, the climate responses in RCP4.5 can be entirely characterized as linear combinations of the fast and slow responses identified in abrupt4$\times$$CO_2$.

We test these assumptions by regressing the annual-mean, multi-model mean surface air temperature anomaly in RCP4.5 (relative to the 1900–1949 historical climate, in K), separately for each year, onto the fast and slow warming patterns (in K K^{-1}; Fig. 3a,b). This yields two regression coefficients that quantify the relative contributions of the fast and slow patterns to the RCP4.5 global-mean temperature anomalies in any given year, plus an intercept which we describe as a residual (Fig. 8b, colored curves). By construction, the regression coefficients and the intercept all have units of K, making their physical interpretation straightforward. Since the fast response occurs within 10 years of the forcing, we expect the fast contribution to warming to closely track the evolution of radiative forcing, while the slow contribution should increase more gradually and continue growing well after the forcing agents stabilize. The regression coefficients are in excellent agreement with our expectation, and the sum of the fast and slow contributions (the "reconstructed" global-mean warming, red curve) closely follows the actual values (Fig. 8b). The coefficient of determination of the regression (R^2) – a measure of the fraction of the spatial variance in the warming pattern that can be explained by our regression model – increases from about 80% in year 2000 to over 95% in year 2050 and beyond. The lower values during the twentieth century could reflect the effects of aerosol forcing on temperature anomaly patterns (next paragraph), but more likely result from the low signal-to-noise ratio during this period when the forcing is still relatively small. From the above results we conclude that to a good approximation, the responses to gradually increasing forcing at any point in time can be understood as a linear combination of fast and slow responses to abrupt CO_2 forcing.

As an aside, we note that during the late twentieth century, the slow contribution grows more rapidly than the fast contribution; this may reflect the mid-century dip in radiative forcing associated with aerosols, to which the fast component responds while the slow component is more sensitive to the cumulative forcing. The partitioning between fast and slow contributions is likely to be less accurate in the mid-twentieth century than in subsequent periods, because the temperature fingerprint of aerosol forcing may not be entirely captured by the fast and slow warming patterns of CO_2. This seems consistent with the regression residual developing during the late twentieth century, and remaining nearly constant thereafter, once the warming becomes dominated by greenhouse gases (purple curve in Fig. 8b). It is also consistent with the low value of R^2 prior to about the year 2000.

b. Contributions of fast and slow responses to RCP4.5 jet shifts

The varying relative importance of the fast and slow patterns of response suggests that the circulation shifts per unit warming should also vary with time in RCP4.5. Since the SH and North Atlantic jets shift only in the fast response, we expect the shifts of these jets to scale with the fast contribution to warming in RCP4.5, and therefore approximately with the radiative forcing, rather than with warming. The North Pacific jet response should depend on both the fast and slow contributions, but should exhibit a more marked equatorward shifting tendency as climate nears equilibrium, when the slow warming pattern becomes more dominant. These predictions can be made quantitative by reconstructing the zonal wind response as a linear combination of the fast and slow patterns (Fig. 3c,d) multiplied by the respective regression coefficients (Fig. 8, middle). It should be borne in mind that this zonal wind reconstruction is entirely based on the patterns of SST change, and therefore it cannot include the effects of stratospheric ozone depletion on the SH jet, as discussed below.

Figure 9 shows the jet latitude as a function of global-mean warming for the actual (black curves) and the reconstructed (red) zonal wind fields. Overall, the jet responses tend to scale more linearly with warming than in abrupt4$\times CO_2$, as expected if the fast and slow time scales of response overlap because of the gradually increasing forcing. However, the SH and North Atlantic jets still show separate time scales of response (black curves in Fig. 9), with an initial poleward shift with warming followed by a stabilization once the forcing has reached its peak (grey vertical bars at year 2080). The zonal wind reconstruction captures these different time scales well (red curves). In the SH, until about 2050 the jet shifts further poleward than would be anticipated based on SST anomaly patterns alone, but this is perfectly consistent with the effect of ozone depletion and recovery (Arblaster and Meehl 2006; Son et al. 2010; McLandress et al. 2011; Barnes et al. 2014). The North Atlantic poleward jet shift is also somewhat overpredicted, but the temporal evolution is well captured by the zonal wind reconstruction. The reconstructed North Pacific jet shift shows no clear response until 2080, followed by a very weak equatorward shift, in agreement with the actual jet behavior. To gain additional insight into the circulation response, we calculate separate jet shift indices for the fast and slow contributions, by using only either the fast or the slow component of the zonal wind change. This confirms that the SH and North Atlantic jet responses are entirely due to the contribution of the fast response to CO_2 forcing – and therefore occur only as long as the radiative forcing keeps increasing – whereas the North Pacific jet remains at a nearly constant latitude owing to competing effects of the fast and slow zonal wind changes.

To fully appreciate the significance of the results in Fig. 9, it is worth keeping in mind that, similar to the abrupt4$\times$$CO_2$ integrations, the RCP4.5 runs have not reached equilibrium by the end of the simulations. Hence substantial further warming could occur beyond year 2300 with no accompanying circulation shift. To highlight this, we approximate the equilibrium warming following the method of Gregory et al. (2004), as described in the Appendix, and calculate the equilibrated jet response under the assumption that all of the long-term warming is associated with the slow pattern.[2] This calculation suggests that the planet would warm by a further 0.75 K beyond

[2]As a caveat, Fig. 7 suggests that at least in CESM, the latter assumption would not be entirely accurate and would lead to an equatorward bias of the North Pacific jet response, for example.

year 2300, with the North Pacific jet shifting slightly equatorward while the SH and North Atlantic jets would remain at near-constant latitude (red dots in Fig. 9). Note that our simple calculation of equilibrium warming likely underestimates the true value (see Appendix). Overall, the clear deviation from linearity in warming indicates that pattern scaling would be a poor assumption to estimate equilibrium circulation responses to greenhouse gas forcing from the transient responses, as discussed in the next section.

5. Discussion and Conclusions

The purpose of this paper is to show that owing to the evolution of spatial patterns of SST increase, the extratropical atmospheric circulation response to greenhouse gas forcing involves two distinct time scales with different characteristics, and consequently midlatitude circulation shifts do not generally scale with global-mean temperature change. Following abrupt CO_2 forcing, poleward circulation shifts occur mainly during the first 5 to 10 years. In subsequent decades, the multi-model mean SH and North Atlantic jets remain at a nearly constant latitude despite substantial global warming, while the North Pacific jet shifts back equatorward. AGCM experiments demonstrate that the two time scales of circulation response are primarily determined by distinct patterns of SST change. "Slow" warming on time scales longer than 10 years is associated with a pattern that has a relatively high degree of low-level polar amplification and is therefore less effective at causing poleward circulation shifts compared with the "fast" warming in the initial 5 to 10 years. In addition to the effect of SSTs, the direct radiative effect of CO_2 also contributes to the fast poleward circulation shift, in line with previous results (Staten et al. 2012; Grise and Polvani 2014). However, the direct response should be restricted to year 1, and therefore cannot account for the bulk of the circulation shift by years 5–10.

Our results imply that poleward circulation shifts generally scale with the cumulative amplitude of the radiative forcing, rather than with the global-mean warming. This is shown to be true in the RCP4.5 experiment, whose response is determined by the same fast and slow patterns as in abrupt4$\times$$CO_2$. Under a scenario in which forcing agents peak and stabilize, we can therefore expect the extratropical circulation to rapidly reach a near-equilibrium, in considerably less time than it takes the climate system to equilibrate. As a corollary, if radiative forcing were to decrease in the future, for example by means of carbon dioxide removal, atmospheric circulation would be expected to respond within a few years. Thus, our results imply that climate change mitigation actions would have a more rapid impact on extratropical atmospheric circulation than on other aspects of climate change related to global-mean temperature.

We have not discussed the seasonality of the time scales of circulation change. In their analysis of the evolution of SH circulation response to CO_2 forcing, Grise and Polvani (2017) found that the jet shift was faster during austral winter than during summer, and the evolution of jet latitude in summer was more similar to that of global-mean temperature. We have analyzed the evolution of SSTs and circulation separately for half-year seasons (November–April and May–October), and found a qualitatively similar evolution in both seasons: the overall features of the fast and slow patterns of SST change show little seasonality, and the majority of the poleward shift occurs within the fast response in each extended season (not shown). In agreement with Grise and Polvani (2017), a weak poleward shift persists in the slow response during austral summer, which these authors ascribe to the evolution of polar lower stratospheric temperature. Hence, the specific character of the slow response may vary seasonally, but the annual-mean perspective is sufficient to demonstrate how the fast and slow time scales in the SST response trigger very different global circulation changes.

Our results suggest that care is warranted when using pattern scaling approaches to estimate atmospheric circulation responses at different levels of equilibration from transient simulations. As an example, the impacts of 2 K global-mean warming – a common policy target (Randalls 2010) – are sometimes assessed by taking a time slice around the time of 2 K warming in transient simulations that are far from reaching steady state (e.g., Schleussner et al. 2016). Applying this method yields an estimated SH jet shift of 1.0°, about two-thirds larger than the estimated *equilibrium* shift of 0.6° for a 2 K warming scenario (calculated by rescaling the equilibrium jet shift in Fig. 9 for a warming of 2 K). Similar errors could occur when using a pattern scaling approach to reconstruct circulation changes under different scenarios with different forcing histories and levels of equilibration. This does not invalidate pattern scaling in general, however; there is no indication based on our results that pattern scaling would not yield accurate results when reconstructing scenarios at similar levels of equilibration.

To conclude, we note that future SST anomaly patterns will have important implications not only for changes in atmospheric circulation and rainfall (Xie et al. 2010; Chadwick et al. 2014), but also for the magnitude of climate feedbacks and therefore climate sensitivity, arguably the most fundamental metric of global climate change (Andrews et al. 2015; Gregory and Andrews 2016; Zhou et al. 2016). Current GCMs predict a wide range of patterns of SST response to greenhouse gas forcing, and our understanding of the responsible processes remains too limited to determine which of these various possible responses are more realistic (Vecchi et al. 2008; Collins et al. 2010; Kohyama and Hartmann 2017). Further work is also needed to test the linearity of the patterns of SST change and their associated time scales, for example by comparing the responses to positive and negative radiative forcing (Held et al. 2010; Good et al. 2016). We hope that our results will motivate further theoretical and observational work to better understand the patterns and time scales of SST change in GCMs.

Acknowledgments. We thank Kevin Grise, Isaac Held, Geoff Vallis, and an anonymous reviewer for helpful comments. We are also grateful to Maria Rugenstein for making available the long CESM ensemble of abrupt4$\times CO_2$ integrations, and for providing comments on the manuscript before submission. This work used the ARCHER UK National Supercomputing Service (http://www.archer.ac.uk), and was supported by the ERC Advanced Grant "ACRCC" (grant number 339390). JMG was supported by the NCAS-Climate program.

APPENDIX

Estimation of the equilibrium global-mean warming in RCP4.5

Here we describe our approach to estimate the equilibrium global-mean warming values shown in Fig. 9. An external forcing F causes a top-of-atmosphere radiative flux imbalance N according to

$$N = F + \lambda \Delta T, \tag{A1}$$

where λ is the feedback parameter (in W m^{-2} K^{-1}), ΔT is the global-mean surface temperature anomaly, and radiative fluxes are positive downward. The feedback parameter λ, which must be negative for a stable system, determines how efficiently the system can restore radiative balance with warming and is treated as a property of the climate model for a given forcing. Once the system has reached equilibrium, $N = 0$ on average, so we may rewrite Equation A1 as $\Delta T_{\text{eq}} = -F_{\text{eq}}/\lambda$, where the subscript "eq" denotes equilibrium values. If the forcing is held constant at its equilibrium value, the values of F_{eq} and λ can be calculated for each model as the intercept and slope of a least-squares fit of annually-averaged values of N versus ΔT (Gregory et al. 2004). We use the N and ΔT time series during 2100–2299, when the forcing agents are held constant and the pattern of SST increase is dominated by the slow response. This yields a multi-model mean equilibrium warming value $\Delta T_{\text{eq}} = 3.86$ K (Fig. 9).

Although we assume the feedback parameter to be a fixed value in our calculation, analyses of coupled atmosphere-ocean CMIP5 GCMs suggest that λ tends to increase (i.e., becomes less negative) over time in abrupt4$\times CO_2$ simulations in most models (Andrews et al. 2012, 2015). As a result, the values of λ calculated by the method of Gregory et al. (2004) may underestimate the effective feedback values, which would result in underestimated equilibrium warming values in Fig. 9. These values should therefore be taken as a likely lower bound for the equilibrium warming in RCP4.5.

References

Andrews, T., J. M. Gregory, and M. J. Webb, 2015: The Dependence of Radiative Forcing and Feedback on Evolving Patterns of Surface Temperature Change in Climate Models. *Journal of Climate*, **28 (4)**, 1630–1648, doi:10.1175/JCLI-D-14-00545.1, URL http://journals.ametsoc.org/doi/abs/10.1175/JCLI-D-14-00545.1.

Andrews, T., J. M. Gregory, M. J. Webb, and K. E. Taylor, 2012: Forcing, feedbacks and climate sensitivity in CMIP5 coupled atmosphere-ocean climate models. *Geophysical Research Letters*, **39 (9)**, L09 712, doi:10.1029/2012GL051607, URL http://doi.wiley.com/10.1029/2012GL051607.

Arblaster, J. M., and G. A. Meehl, 2006: Contributions of External Forcings to Southern Annular Mode Trends. *Journal of Climate*, **19 (12)**, 2896–2905, doi:10.1175/JCLI3774.1, URL http://journals.ametsoc.org/doi/abs/10.1175/JCLI3774.1.

Armour, K. C., C. M. Bitz, and G. H. Roe, 2013: Time-Varying Climate Sensitivity from Regional Feedbacks. *Journal of Climate*, **26 (13)**, 4518–4534, doi:10.1175/JCLI-D-12-00544.1, URL http://journals.ametsoc.org/doi/abs/10.1175/JCLI-D-12-00544.1.

Armour, K. C., J. Marshall, J. R. Scott, A. Donohoe, and E. R. Newsom, 2016: Southern Ocean warming delayed by circumpolar upwelling and equatorward transport. *Nature Geoscience*, **9 (7)**, 549–554, doi:10.1038/ngeo2731, URL http://www.nature.com/doifinder/10.1038/ngeo2731.

Barnes, E. A., N. W. Barnes, and L. M. Polvani, 2014: Delayed Southern Hemisphere Climate Change Induced by Stratospheric Ozone Recovery, as Projected by the CMIP5 Models. *Journal of Climate*, **27 (2)**, 852–867, doi:10.1175/JCLI-D-13-00246.1, URL http://journals.ametsoc.org/doi/abs/10.1175/JCLI-D-13-00246.1.

Barnes, E. A., and L. Polvani, 2013: Response of the midlatitude jets and of their variability to increased greenhouse gases in the CMIP5 models. *Journal of Climate*, **26 (18)**, 7117–7135, doi:10.1175/JCLI-D-12-00536.1, URL http://journals.ametsoc.org/doi/abs/10.1175/JCLI-D-12-00536.1.

Bjerknes, J., 1969: Atmospheric Teleconnections from the Equatorial Pacific. *Monthly Weather Review*, **97 (3)**, 163–172, doi:10.1175/1520-0493(1969)097⟨0163:ATFTEP⟩2.3.CO;2, URL http://journals.ametsoc.org/doi/abs/10.1175/1520-0493{\%}281969{\%}29097{\%}3C0163{\%}3AATFTEP{\%}3E2.3.CO{\%}3B2.

Bony, S., G. Bellon, D. Klocke, S. Sherwood, S. Fermepin, and S. Denvil, 2013: Robust direct effect of carbon dioxide on tropical circulation and regional precipitation. *Nature Geoscience*, **6 (6)**, 447–451, doi:10.1038/ngeo1799, URL http://www.nature.com/doifinder/10.1038/ngeo1799.

Brayshaw, D. J., B. Hoskins, and M. Blackburn, 2008: The Storm-Track Response to Idealized SST Perturbations in an Aquaplanet GCM. *Journal of the Atmospheric Sciences*,

65 (9), 2842–2860, doi:10.1175/2008JAS2657.1, URL http://journals.ametsoc.org/doi/abs/10.1175/2008JAS2657.1.

Butler, A. H., D. W. J. Thompson, and R. Heikes, 2010: The Steady-State Atmospheric Circulation Response to Climate Change–like Thermal Forcings in a Simple General Circulation Model. *Journal of Climate*, **23 (13)**, 3474–3496, URL http://journals.ametsoc.org/doi/abs/10.1175/2010JCLI3228.1.

Caldwell, P. M., M. D. Zelinka, K. E. Taylor, and K. Marvel, 2016: Quantifying the Sources of Intermodel Spread in Equilibrium Climate Sensitivity. *Journal of Climate*, **29 (2)**, 513–524, doi:10.1175/JCLI-D-15-0352.1, URL http://journals.ametsoc.org/doi/10.1175/JCLI-D-15-0352.1.

Ceppi, P., and D. L. Hartmann, 2016: Clouds and the Atmospheric Circulation Response to Warming. *Journal of Climate*, **29 (2)**, 783–799, doi:10.1175/JCLI-D-15-0394.1, URL http://journals.ametsoc.org/doi/10.1175/JCLI-D-15-0394.1.

Ceppi, P., Y.-T. Hwang, X. Liu, D. M. W. Frierson, and D. L. Hartmann, 2013: The relationship between the ITCZ and the Southern Hemispheric eddy-driven jet. *Journal of Geophysical Research: Atmospheres*, **118 (11)**, 5136–5146, doi:10.1002/jgrd.50461, URL http://doi.wiley.com/10.1002/jgrd.50461.

Ceppi, P., M. D. Zelinka, and D. L. Hartmann, 2014: The response of the Southern Hemispheric eddy-driven jet to future changes in shortwave radiation in CMIP5. *Geophysical Research Letters*, **41 (9)**, 3244–3250, doi:10.1002/2014GL060043, URL http://doi.wiley.com/10.1002/2014GL060043.

Chadwick, R., P. Good, T. Andrews, and G. Martin, 2014: Surface warming patterns drive tropical rainfall pattern responses to CO₂ forcing on all timescales. *Geophysical*

Research Letters, **41 (2)**, 610–615, doi:10.1002/2013GL058504, URL http://doi.wiley.com/10.1002/2013GL058504.

Chang, E. K. M., Y. Guo, and X. Xia, 2012: CMIP5 multimodel ensemble projection of storm track change under global warming. *Journal of Geophysical Research*, **117 (D23)**, D23 118, doi:10.1029/2012JD018578, URL http://doi.wiley.com/10.1029/2012JD018578.

Chen, G., J. Lu, and D. M. W. Frierson, 2008: Phase Speed Spectra and the Latitude of Surface Westerlies: Interannual Variability and Global Warming Trend. *Journal of Climate*, **21 (22)**, 5942–5959, doi:10.1175/2008JCLI2306.1, URL http://journals.ametsoc.org/doi/abs/10.1175/2008JCLI2306.1.

Chen, G., R. A. Plumb, and J. Lu, 2010: Sensitivities of zonal mean atmospheric circulation to SST warming in an aqua-planet model. *Geophysical Research Letters*, **37 (12)**, L12 701, doi:10.1029/2010GL043473, URL http://onlinelibrary.wiley.com/doi/10.1029/2010GL043473/abstract.

Clement, A. C., R. Seager, M. A. Cane, and S. E. Zebiak, 1996: An Ocean Dynamical Thermostat. *Journal of Climate*, **9 (9)**, 2190–2196, doi:10.1175/1520-0442(1996)009⟨2190:AODT⟩2.0.CO;2, URL http://journals.ametsoc.org/doi/abs/10.1175/1520-0442{\%}281996{\%}29009{\%}3C2190{\%}3AAODT{\%}3E2.0.CO{\%}3B2.

Collins, M., and Coauthors, 2005: El Niño- or La Niña-like climate change? *Climate Dynamics*, **24 (1)**, 89–104, doi:10.1007/s00382-004-0478-x, URL http://link.springer.com/10.1007/s00382-004-0478-x.

Collins, M., and Coauthors, 2010: The impact of global warming on the tropical Pacific Ocean and El Niño. *Nature Geoscience*, **3 (6)**, 391–397, doi:10.1038/ngeo868, URL http://www.nature.

com/doifinder/10.1038/ngeo868.

Collins, M., and Coauthors, 2013: Long-term Climate Change: Projections, Commitments and Irreversibility. *Climate Change 2013: The Physical Science Basis. Contribution of Working Group I to the Fifth Assessment Report of the Intergovernmental Panel on Climate Change*, T. F. Stocker, D. Qin, G.-K. Plattner, M. Tignor, S. K. Allen, J. Boschung, A. Nauels, Y. Xia, V. Bex, and P. M. Midgley, Eds., Cambridge University Press, Cambridge, United Kingdom and New York, NY, USA, 1029–1136.

Delcambre, S. C., D. J. Lorenz, D. J. Vimont, and J. E. Martin, 2013: Diagnosing Northern Hemisphere Jet Portrayal in 17 CMIP3 Global Climate Models: Twenty-First-Century Projections. *Journal of Climate*, **26 (14)**, 4930–4946, doi:10.1175/JCLI-D-12-00359.1, URL http://journals.ametsoc.org/doi/abs/10.1175/JCLI-D-12-00359.1.

Deser, C., and A. S. Phillips, 2009: Atmospheric Circulation Trends, 19502000: The Relative Roles of Sea Surface Temperature Forcing and Direct Atmospheric Radiative Forcing. *Journal of Climate*, **22 (2)**, 396–413, doi:10.1175/2008JCLI2453.1, URL http://journals.ametsoc.org/doi/abs/10.1175/2008JCLI2453.1.

Dickinson, R. E., 1981: Convergence Rate and Stability of Ocean-Atmosphere Coupling Schemes with a Zero-Dimensional Climate Model. *Journal of the Atmospheric Sciences*, **38 (10)**, 2112–2120, doi:10.1175/1520-0469(1981)038⟨2112:CRASOO⟩2.0.CO;2, URL http://journals.ametsoc.org/doi/abs/10.1175/1520-0469{\%}281981{\%}29038{\%}3C2112{\%}3ACRASOO{\%}3E2.0.CO{\%}3B2.

Drijfhout, S., G. J. van Oldenborgh, and A. Cimatoribus, 2012: Is a Decline of AMOC Causing the Warming Hole above the North Atlantic in Observed and Modeled Warming Patterns? *Journal of Climate*, **25 (24)**, 8373–8379, doi:10.1175/JCLI-D-12-00490.1, URL http://journals.ametsoc.org/doi/abs/10.1175/JCLI-D-12-00490.1.

Geoffroy, O., and D. Saint-Martin, 2014: Pattern decomposition of the transient climate response. *Tellus A: Dynamic Meteorology and Oceanography*, **66 (1)**, 23 393, doi:10.3402/tellusa.v66.23393, URL https://www.tandfonline.com/doi/full/10.3402/tellusa.v66.23393.

Geoffroy, O., D. Saint-Martin, D. J. L. Olivié, A. Voldoire, and G. Bellon, 2013: Transient Climate Response in a Two-Layer Energy-Balance Model. Part I: Analytical Solution and Parameter Calibration Using CMIP5 AOGCM Experiments. *Journal of Climate*, **26 (6)**, 1841–1857, doi:10.1175/JCLI-D-12-00195.1, URL http://journals.ametsoc.org/doi/abs/10.1175/JCLI-D-12-00195.1.

Good, P., T. Andrews, R. Chadwick, J.-L. Dufresne, J. M. Gregory, J. A. Lowe, N. Schaller, and H. Shiogama, 2016: nonlinMIP contribution to CMIP6: model intercomparison project for non-linear mechanisms: physical basis, experimental design and analysis principles (v1.0). *Geoscientific Model Development*, **9 (11)**, 4019–4028, doi:10.5194/gmd-9-4019-2016, URL http://www.geosci-model-dev.net/9/4019/2016/.

Good, P., J. M. Gregory, and J. A. Lowe, 2011: A step-response simple climate model to reconstruct and interpret AOGCM projections. *Geophysical Research Letters*, **38 (1)**, n/a–n/a, doi:10.1029/2010GL045208, URL http://doi.wiley.com/10.1029/2010GL045208.

Good, P., J. M. Gregory, J. A. Lowe, and T. Andrews, 2013: Abrupt CO2 experiments as tools for predicting and understanding CMIP5 representative concentration pathway projections. *Climate Dynamics*, **40 (3-4)**, 1041–1053, doi:10.1007/s00382-012-1410-4, URL http://link.springer.com/10.1007/s00382-012-1410-4.

Gregory, J. M., 2000: Vertical heat transports in the ocean and their effect on time-dependent climate change. *Climate Dynamics*, **16 (7)**, 501–515, doi:10.1007/s003820000059, URL http://link.springer.com/10.1007/s003820000059.

Gregory, J. M., and T. Andrews, 2016: Variation in climate sensitivity and feedback parameters during the historical period. *Geophysical Research Letters*, **43 (8)**, 3911–3920, doi:10.1002/2016GL068406, URL http://doi.wiley.com/10.1002/2016GL068406.

Gregory, J. M., and Coauthors, 2004: A new method for diagnosing radiative forcing and climate sensitivity. *Geophysical Research Letters*, **31 (3)**, L03 205, doi:10.1029/2003GL018747, URL http://doi.wiley.com/10.1029/2003GL018747.

Grise, K. M., and L. M. Polvani, 2014: The response of midlatitude jets to increased CO₂ : Distinguishing the roles of sea surface temperature and direct radiative forcing. *Geophysical Research Letters*, **41 (19)**, 6863–6871, doi:10.1002/2014GL061638, URL http://doi.wiley.com/10.1002/2014GL061638.

Grise, K. M., and L. M. Polvani, 2017: Understanding the timescales of the tropospheric circulation response to abrupt CO2 forcing in the Southern Hemisphere: Seasonality and the role of the stratosphere. *Journal of Climate*, doi:10.1175/JCLI-D-16-0849.1.

Harvey, B. J., L. C. Shaffrey, and T. J. Woollings, 2014: Equator-to-pole temperature differences and the extra-tropical storm track responses of the CMIP5 climate models. *Climate Dynamics*, **43 (5-6)**, 1171–1182, doi:10.1007/s00382-013-1883-9, URL http://link.springer.com/10.1007/s00382-013-1883-9.

Held, I. M., M. Winton, K. Takahashi, T. Delworth, F. Zeng, and G. K. Vallis, 2010: Probing the Fast and Slow Components of Global Warming by Returning Abruptly to Preindustrial Forcing. *Journal of Climate*, **23 (9)**, 2418–2427, doi:10.1175/2009JCLI3466.1, URL http://journals.ametsoc.org/doi/abs/10.1175/2009JCLI3466.1.

Hurrell, J. W., and Coauthors, 2013: The Community Earth System Model: A Framework for Collaborative Research. *Bulletin of the American Meteorological Society*, **94 (9)**, 1339–1360, doi:10.1175/BAMS-D-12-00121.1, URL http://journals.ametsoc.org/doi/abs/10.1175/BAMS-D-12-00121.1.

Kang, S. M., and L. M. Polvani, 2011: The Interannual Relationship between the Latitude of the Eddy-Driven Jet and the Edge of the Hadley Cell. *Journal of Climate*, **24 (2)**, 563–568, doi:10.1175/2010JCLI4077.1, URL http://journals.ametsoc.org/doi/abs/10.1175/2010JCLI4077.1.

Kohyama, T., and D. L. Hartmann, 2016: Antarctic Sea Ice Response to Weather and Climate Modes of Variability. *Journal of Climate*, **29 (2)**, 721–741, doi:10.1175/JCLI-D-15-0301.1, URL http://journals.ametsoc.org/doi/10.1175/JCLI-D-15-0301.1.

Kohyama, T., and D. L. Hartmann, 2017: Nonlinear ENSO Warming Suppression (NEWS). *Journal of Climate*, doi:10.1175/JCLI-D-16-0541.1, URL http://journals.ametsoc.org/doi/10.1175/JCLI-D-16-0541.1.

Kushner, P. J., I. M. Held, and T. L. Delworth, 2001: Southern Hemisphere Atmospheric Circulation Response to Global Warming. *Journal of Climate*, **14 (10)**, 2238–2249, doi:10.1175/1520-0442(2001)014⟨0001:SHACRT⟩2.0.CO;2, URL http://journals.ametsoc.org/doi/abs/10.1175/1520-0442(2001)014{\%}3C0001:SHACRT{\%}3E2.0.CO;2.

Long, S.-M., S.-P. Xie, X.-T. Zheng, and Q. Liu, 2014: Fast and Slow Responses to Global Warming: Sea Surface Temperature and Precipitation Patterns. *Journal of Climate*, **27 (1)**, 285–299, doi:10.1175/JCLI-D-13-00297.1, URL http://journals.ametsoc.org/doi/abs/10.1175/JCLI-D-13-00297.1.

Lu, J., G. A. Vecchi, and T. Reichler, 2007: Expansion of the Hadley cell under global warming. *Geophysical Research Letters*, **34 (6)**, L06 805, doi:10.1029/2006GL028443, URL http://www.agu.org/pubs/crossref/2007/2006GL028443.shtml.

Manabe, S., K. Bryan, and M. J. Spelman, 1990: Transient Response of a Global Ocean-Atmosphere Model to a Doubling of Atmospheric Carbon Dioxide. *Journal of Physical Oceanography*, **20 (5)**, 722–749, doi:10.1175/1520-0485(1990)020⟨0722:TROAGO⟩2.0.CO;2, URL http://journals.ametsoc.org/doi/abs/10.1175/1520-0485{\%}281990{\%}29020{\%}3C0722{\%}3ATROAGO{\%}3E2.0.CO{\%}3B2.

Manabe, S., R. J. Stouffer, M. J. Spelman, and K. Bryan, 1991: Transient Responses of a Coupled OceanAtmosphere Model to Gradual Changes of Atmospheric CO₂. Part I. Annual Mean Response. *Journal of Climate*, **4 (8)**, 785–818, doi:10.1175/1520-0442(1991)004⟨0785:TROACO⟩2.0.CO;2, URL http://journals.ametsoc.org/doi/abs/10.1175/1520-0442{\%}281991{\%}29004{\%}3C0785{\%}3ATROACO{\%}3E2.0.CO{\%}3B2.

McLandress, C., T. G. Shepherd, J. F. Scinocca, D. A. Plummer, M. Sigmond, A. I. Jonsson, and M. C. Reader, 2011: Separating the Dynamical Effects of Climate Change and Ozone Depletion. Part II: Southern Hemisphere Troposphere. *Journal of Climate*, **24 (6)**, 1850–1868, doi:10.1175/2010JCLI3958.1, URL http://journals.ametsoc.org/doi/abs/10.1175/2010JCLI3958.1.

Meinshausen, M., and Coauthors, 2011: The RCP greenhouse gas concentrations and their extensions from 1765 to 2300. *Climatic Change*, **109 (1-2)**, 213–241, doi:10.1007/s10584-011-0156-z, URL http://link.springer.com/10.1007/s10584-011-0156-z.

Mitchell, T. D., 2003: Pattern Scaling: An Examination of the Accuracy of the Technique for Describing Future Climates. *Climatic Change*, **60 (3)**, 217–242, doi:10.1023/A:1026035305597, URL http://link.springer.com/10.1023/A:1026035305597.

Neale, R. B., and Coauthors, 2010: Description of the NCAR Community Atmosphere Model (CAM 4.0). *NCAR Tech. Note TN-485*, NCAR, 212.

Olivié, D. J. L., G. P. Peters, and D. Saint-Martin, 2012: Atmosphere Response Time Scales Estimated from AOGCM Experiments. *Journal of Climate*, **25 (22)**, 7956–7972, doi:10.1175/JCLI-D-11-00475.1, URL http://journals.ametsoc.org/doi/abs/10.1175/JCLI-D-11-00475.1.

Randalls, S., 2010: History of the 2 C climate target. *Wiley Interdisciplinary Reviews: Climate Change*, **1 (4)**, 598–605, doi:10.1002/wcc.62, URL http://doi.wiley.com/10.1002/wcc.62.

Rugenstein, M. A. A., J. M. Gregory, N. Schaller, J. Sedláček, and R. Knutti, 2016a: Multi-annual ocean-atmosphere adjustments to radiative forcing. *Journal of Climate*, JCLI–D–16–0312.1, doi:10.1175/JCLI-D-16-0312.1, URL http://journals.ametsoc.org/doi/abs/10.1175/JCLI-D-16-0312.1.

Rugenstein, M. A. A., J. Sedláček, and R. Knutti, 2016b: Nonlinearities in patterns of long-term ocean warming. *Geophysical Research Letters*, **43 (7)**, 3380–3388, doi:10.1002/2016GL068041, URL http://doi.wiley.com/10.1002/2016GL068041.

Santer, B. D., T. M. Wigley, M. E. Schlesinger, and J. F. Mitchell, 1990: Developing climate scenarios from equilibrium GCM results. Tech. rep., Max-Planck-Institut für Meteorologie, Hamburg, 1–29 pp.

Schleussner, C.-F., and Coauthors, 2016: Differential climate impacts for policy-relevant limits to global warming: the case of 1.5C and 2C. *Earth System Dynamics*, **7 (2)**, 327–351, doi: 10.5194/esd-7-327-2016, URL http://www.earth-syst-dynam.net/7/327/2016/.

Simpson, I. R., T. A. Shaw, and R. Seager, 2014: A Diagnosis of the Seasonally and Longitudinally Varying Midlatitude Circulation Response to Global Warming. *Journal of the Atmospheric Sciences*, **71 (7)**, 2489–2515, doi:10.1175/JAS-D-13-0325.1, URL http://journals.ametsoc.org/doi/abs/10.1175/JAS-D-13-0325.1.

Son, S.-W., and Coauthors, 2010: Impact of stratospheric ozone on Southern Hemisphere circulation change: A multimodel assessment. *Journal of Geophysical Research*, **115 (D3)**, D00M07, doi:10.1029/2010JD014271, URL http://doi.wiley.com/10.1029/2010JD014271.

Staten, P. W., J. J. Rutz, T. Reichler, and J. Lu, 2012: Breaking down the tropospheric circulation response by forcing. *Climate Dynamics*, **39 (9)**, 2361–2375, doi:10.1007/s00382-011-1267-y, URL http://www.springerlink.com/content/d2458600863q2567/.

Stouffer, R. J., 2004: Time Scales of Climate Response. *Journal of Climate*, **17 (1)**, 209–217, doi:10.1175/1520-0442(2004)017⟨0209:TSOCR⟩2.0.CO;2, URL http://journals.ametsoc.org/doi/abs/10.1175/1520-0442{\%}282004{\%}29017{\%}3C0209{\%}3ATSOCR{\%}3E2.0.CO{\%}3B2.

Taylor, K. E., R. J. Stouffer, and G. A. Meehl, 2012: An Overview of CMIP5 and the Experiment Design. *Bulletin of the American Meteorological Society*, **93 (4)**, 485–498, doi:10.1175/BAMS-D-11-00094.1, URL http://journals.ametsoc.org/doi/abs/10.1175/BAMS-D-11-00094.1.

Tebaldi, C., and J. M. Arblaster, 2014: Pattern scaling: Its strengths and limitations, and an update on the latest model simulations. *Climatic Change*, **122 (3)**, 459–471, doi:10.1007/s10584-013-1032-9, URL http://link.springer.com/10.1007/s10584-013-1032-9.

Vallis, G. K., P. Zurita-Gotor, C. Cairns, and J. Kidston, 2015: Response of the large-scale structure of the atmosphere to global warming. *Quarterly Journal of the Royal Meteorological Society*, **141 (690)**, 1479–1501, doi:10.1002/qj.2456, URL http://doi.wiley.com/10.1002/qj.2456.

Vecchi, G. A., A. Clement, and B. J. Soden, 2008: Examining the Tropical Pacific's Response to Global Warming. *Eos, Transactions American Geophysical Union*, **89 (9)**, 81–83, doi:10.1029/2008EO090002, URL http://doi.wiley.com/10.1029/2008EO090002.

Wang, H., S.-P. Xie, and Q. Liu, 2016: Comparison of Climate Response to Anthropogenic Aerosol versus Greenhouse Gas Forcing: Distinct Patterns. *Journal of Climate*, **29 (14)**, 5175–5188, doi:10.1175/JCLI-D-16-0106.1, URL http://journals.ametsoc.org/doi/10.1175/JCLI-D-16-0106.1.

Woollings, T., J. M. Gregory, J. G. Pinto, M. Reyers, and D. J. Brayshaw, 2012: Response of the North Atlantic storm track to climate change shaped by ocean-atmosphere coupling. *Nature Geoscience*, **5 (5)**, 313–317, doi:10.1038/ngeo1438, URL http://www.nature.com/doifinder/10.1038/ngeo1438.

Wu, Y., R. Seager, T. A. Shaw, M. Ting, and N. Naik, 2013: Atmospheric Circulation Response to an Instantaneous Doubling of Carbon Dioxide. Part II: Atmospheric Transient Adjustment and Its Dynamics. *Journal of Climate*, **26 (3)**, 918–935, doi:10.1175/JCLI-D-12-00104.1, URL http://journals.ametsoc.org/doi/abs/10.1175/JCLI-D-12-00104.1.

Xie, S.-P., C. Deser, G. A. Vecchi, J. Ma, H. Teng, and A. T. Wittenberg, 2010: Global Warming Pattern Formation: Sea Surface Temperature and Rainfall. *Journal of Climate*, **23 (4)**, 966–986, doi:10.1175/2009JCLI3329.1, URL http://journals.ametsoc.org/doi/abs/10.1175/2009JCLI3329.1.

Xie, S.-P., B. Lu, and B. Xiang, 2013: Similar spatial patterns of climate responses to aerosol and greenhouse gas changes. *Nature Geoscience*, **6 (10)**, 828–832, doi:10.1038/ngeo1931, URL http://www.nature.com/doifinder/10.1038/ngeo1931.

Xie, S.-P., and S. G. H. Philander, 1994: A coupled ocean-atmosphere model of relevance to the ITCZ in the eastern Pacific. *Tellus A*, **46 (4)**, 340–350, doi:10.1034/j.1600-0870.1994.t01-1-00001.x, URL http://tellusa.net/index.php/tellusa/article/view/15484.

Yin, J. H., 2005: A consistent poleward shift of the storm tracks in simulations of 21st century climate. *Geophysical Research Letters*, **32 (18)**, L18 701, doi:10.1029/2005GL023684, URL http://onlinelibrary.wiley.com/doi/10.1029/2005GL023684/abstract.

Zhou, C., M. D. Zelinka, and S. A. Klein, 2016: Impact of decadal cloud variations on the Earth's energy budget. *Nature Geoscience*, **9 (12)**, 871–874, doi:10.1038/ngeo2828, URL http://www.nature.com/doifinder/10.1038/ngeo2828.

LIST OF TABLES

TABLE 1. List of CMIP5 models used in the analysis. Crosses indicate available data for the respective experiments.

Model name	piControl & abrupt4×CO_2	historical & RCP4.5
ACCESS1.0	×	
ACCESS1.3	×	
BCC-CSM1.1	×	×
BCC-CSM1.1(m)	×	
BNU-ESM	×	
CanESM2	×	×
CCSM4	×	×
CNRM-CM5	×	×
CSIRO-Mk3.6.0	×	×
FGOALS-g2	×	
FGOALS-s2	×	
GFDL-CM3	×	
GFDL-ESM2G	×	
GFDL-ESM2M	×	
GISS-E2-H	×	×
GISS-E2-R	×	×
HadGEM2-ES	×	
INM-CM4	×	
IPSL-CM5A-LR	×	×
IPSL-CM5A-MR	×	×
IPSL-CM5B-LR	×	
MIROC5	×	
MIROC-ESM	×	×
MPI-ESM-LR	×	×
MPI-ESM-MR	×	
MPI-ESM-P	×	
MRI-CGCM3	×	
NorESM1-M	×	×

LIST OF FIGURES

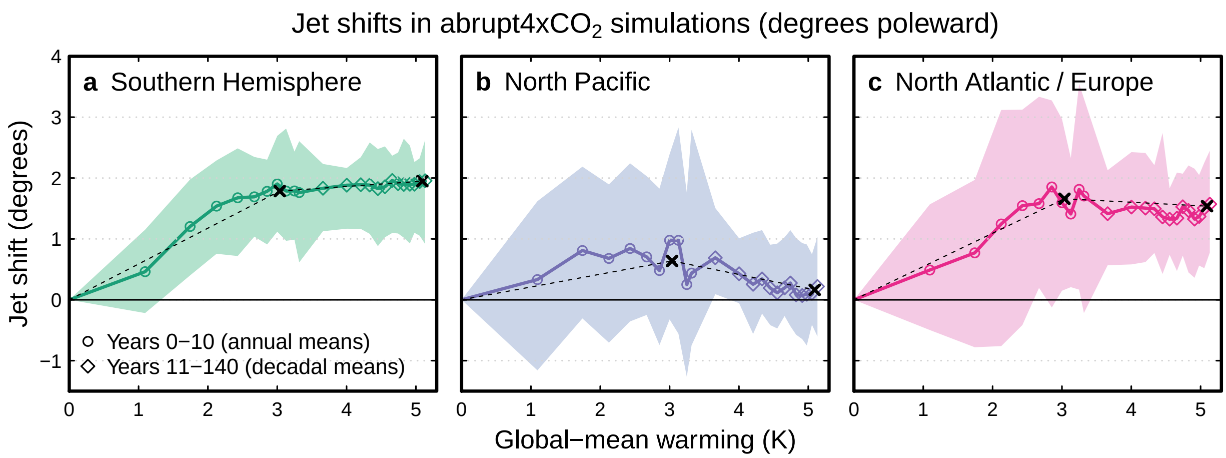

FIG. 1. Jet shifts in abrupt4$\times CO_2$ integrations as a function of global-mean surface air temperature anomaly. The curves denote multi-model means, while shading indicates the 75% range (12.5 to 87.5 percentiles of the distribution) of model values. Annual-mean values are shown for years 1–10 (circles) and decadal-mean values for years 11–140 (diamonds). Black crosses indicate the means for years 5–10 and 121–140, and dashed lines represent linearly interpolated values between these points. Zonal wind values are ensemble-averaged year by year prior to calculating jet indices, and are plotted against the multi-model mean temperature.

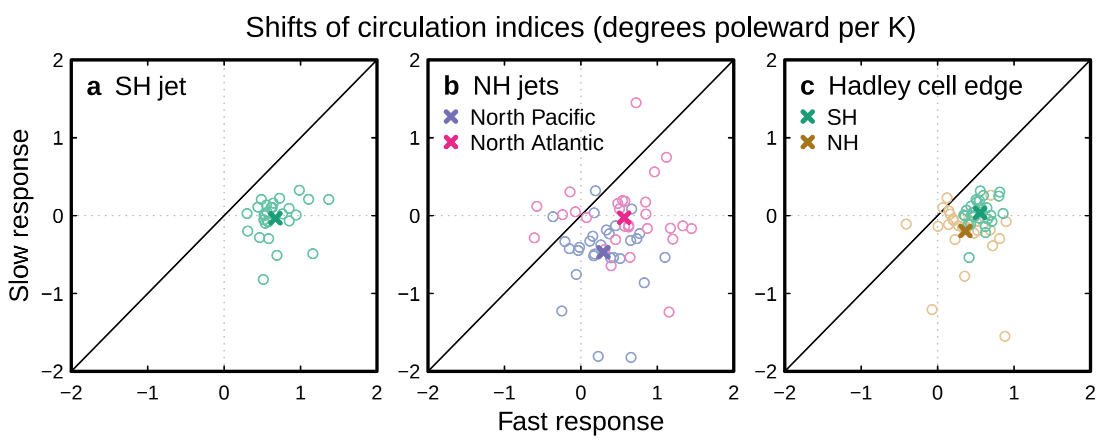

FIG. 2. Fast and slow atmospheric circulation responses to warming in individual models (open circles) and in the multi-model mean (thick crosses). The fast response is defined as the difference in climate between the pre-industrial control and years 5–10, while the slow response is the change between years 5–10 and 121–140.

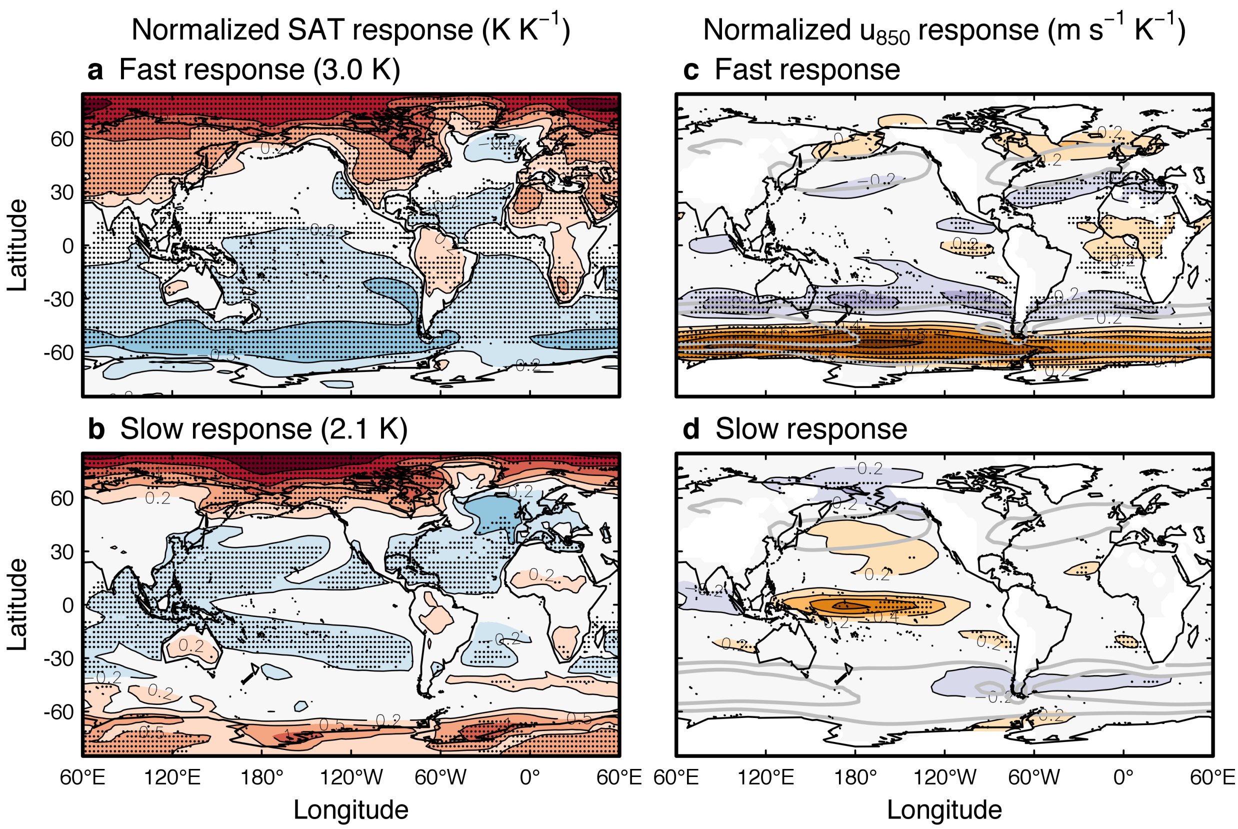

FIG. 3. Multi-model mean patterns of change in surface air temperature (left) and 850 hPa zonal wind (right) in abrupt4$\times CO_2$, all normalized by global-mean warming during the respective periods. To highlight the spatial patterns, we subtract 1 from the temperature patterns to yield a global-mean of 0. Thick grey contours denote the control zonal wind climatology (contours at 5 and 10 m s^{-1}). Areas where 90% of the models agree on the sign of the response are stippled.

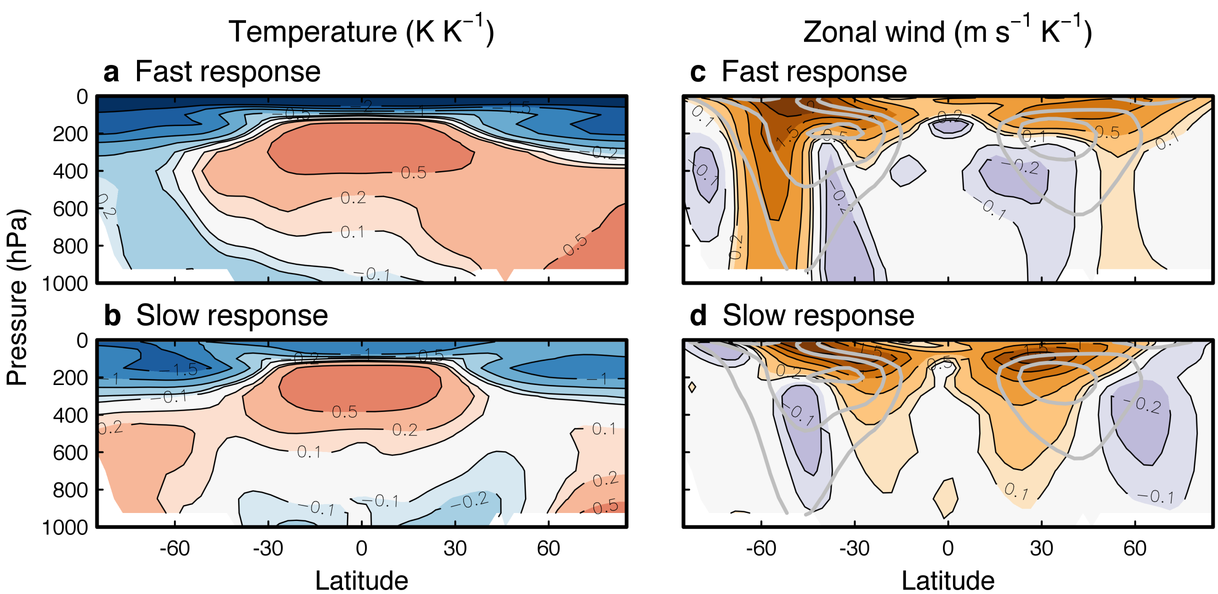

FIG. 4. As in Fig. 3, but for zonal-mean temperature and zonal wind. The global-mean temperature response has been subtracted at each level. Thick grey contours denote the control zonal wind climatology (contours at 10, 20, and 30 m s^{-1}).

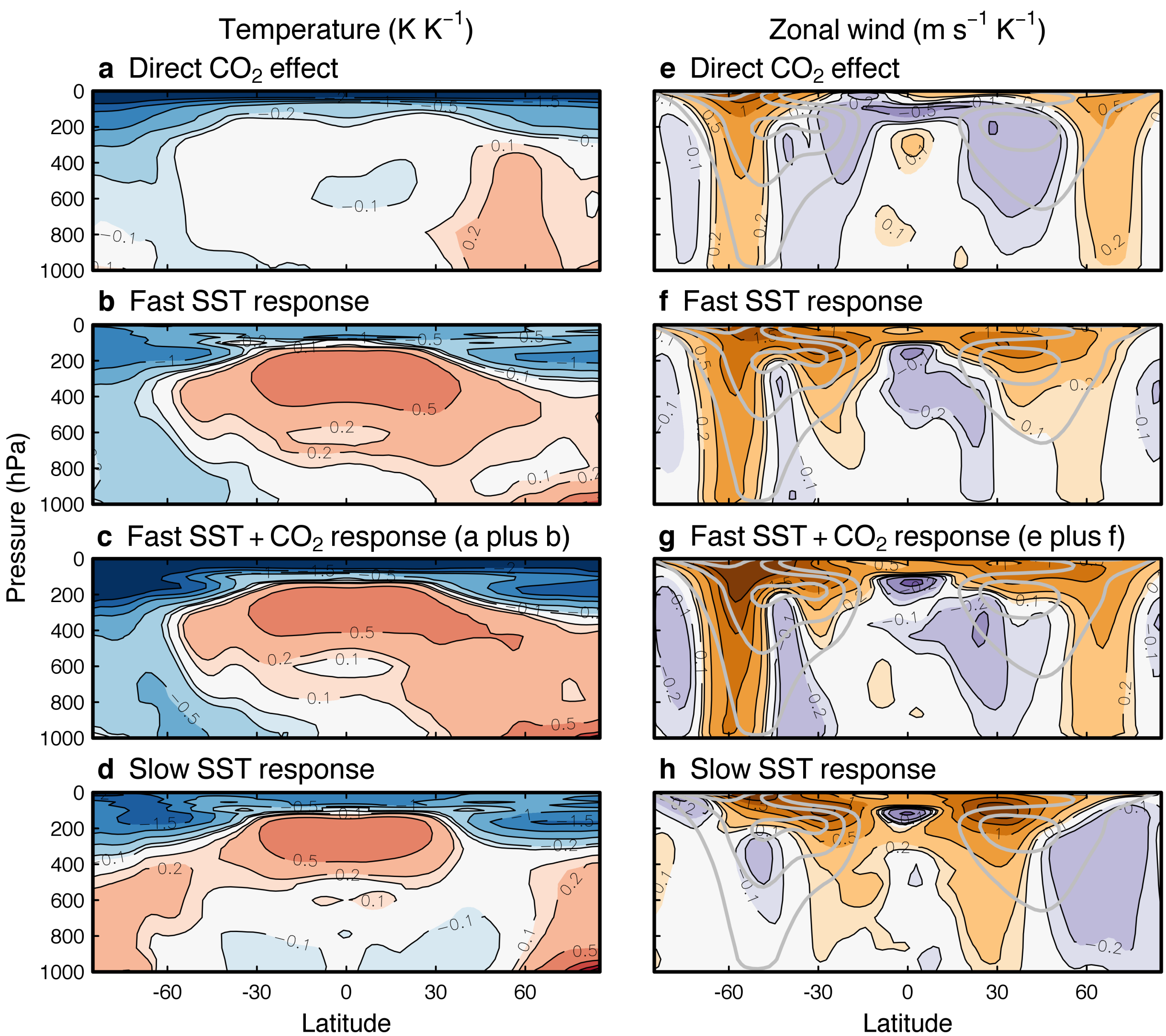

807 FIG. 5. As in Fig. 4, but for CAM4 AGCM experiments. Panels a, b, e, and f are all normalized by the
808 combined global-mean surface warming due to CO_2 forcing and fast SST pattern, so that the sum of the first two
809 rows equals the third row.

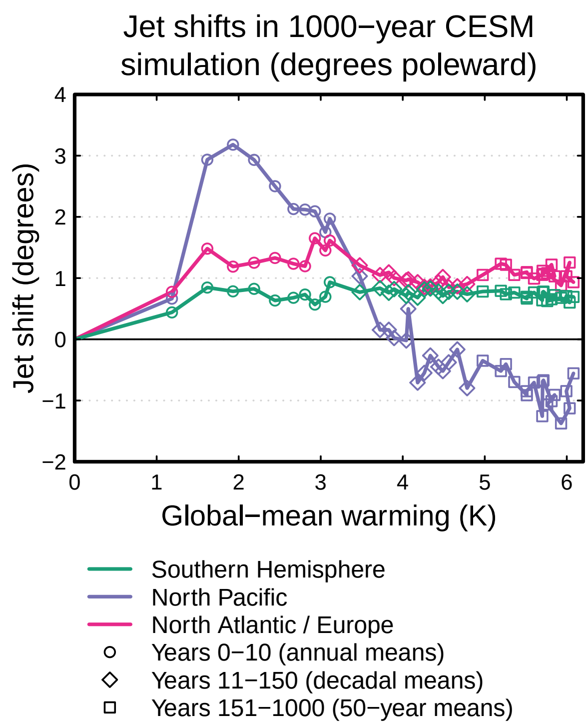

FIG. 6. Jet shifts as a function of global-mean surface warming in a 1000-year abrupt4$\times$$CO_2$ experiment with CESM. Decadal-mean values are shown for years 11-150 (diamonds) and 50-year means for years 151-1000 (squares). The values are ensemble averages up to year 250 (see text).

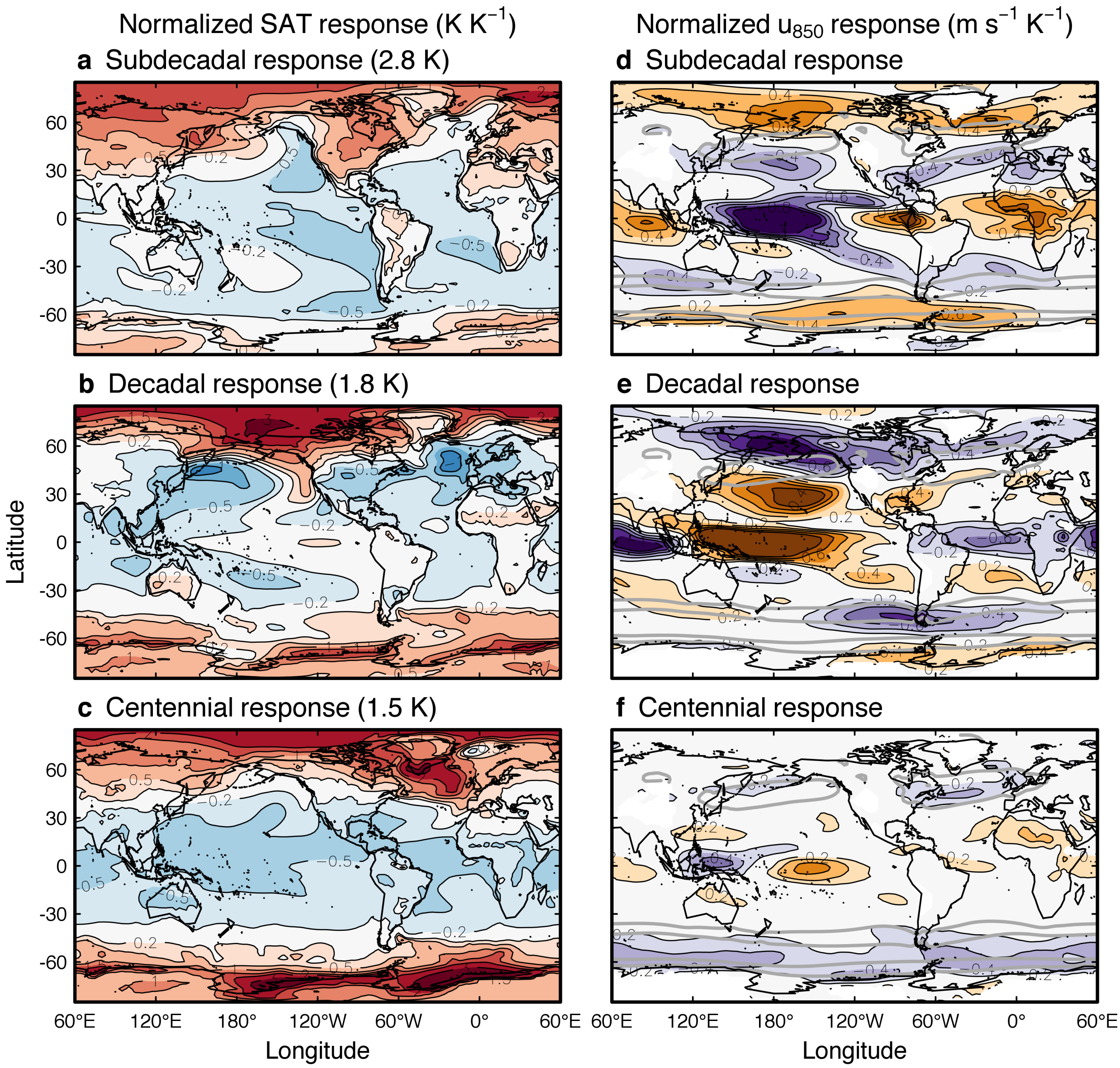

FIG. 7. As in Fig. 3, but for the 1000-year CESM abrupt4$\times CO_2$ experiment. The subdecadal and decadal responses correspond to the fast and slow responses in Fig. 3. The centennial response (panels c, f) is defined as the normalized difference between years 121-140 and 951-1000.

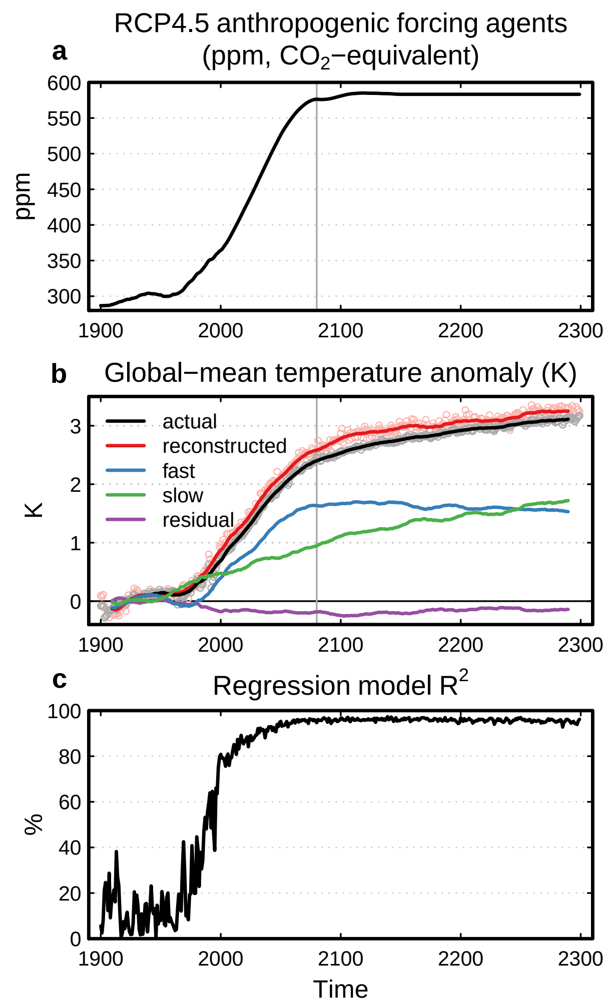

FIG. 8. (a) Time series of CO_2-equivalent concentration of anthropogenic forcing agents, (b) global-mean, multi-model mean surface temperature anomaly in RCP4.5, relative to the 1900-1949 climatology, and (c) coefficient of determination (R^2) from the regression model. The vertical grey bar in panels a–b indicates year 2080, at which point atmospheric CO_2 concentration approximately stabilizes.

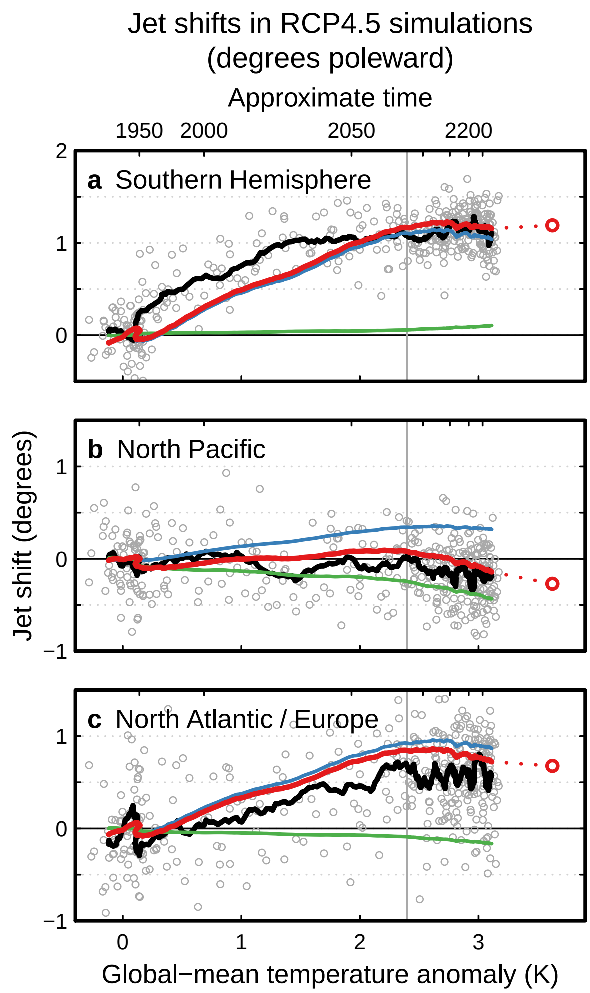

820 FIG. 9. Jet shifts in RCP4.5 as a function of global-mean warming. Open circles denote individual years, while the black curves show 20-year running averages. The red curve is the reconstructed jet latitude evolution, and the open red circle indicates the estimated equilibrium global warming and jet response (see text). Blue and green curves represent the fast and slow warming contributions to jet shifts (see text). The vertical grey bar indicates year 2080, when CO_2 concentration approximately stabilizes.